

# SHEAR FAILURE AT A CRACK TIP UNDER SHEAR WAVE LOADING

Z. ZHANG & R. J. CLIFTON  
Division of Engineering, Brown University, Providence, RI 02912, USA

## ABSTRACT

Pressure-shear plate impact experiments are used to study dynamic failure at a crack tip subjected to shear wave loading. Plane, shear-wave loading of an effectively semi-infinite crack is obtained by the impact of a flyer plate and a pre-cracked target plate having a mid-plane, half-through, fatigue crack that is parallel to the impact face. The flyer and target plates are parallel, but inclined relative to their direction of approach. Normal tractions on the crack faces are eliminated by choosing the flyer thickness to be sufficiently small that the incident longitudinal wave passes through the crack plane before the shear wave arrives. By rotating the target about its cylindrical axis it is possible to subject the crack plane to either Mode II or Mode III loading, or any combination thereof. Herein experimental results are presented for Mode II loading. The results of these experiments are interpreted using 2D finite element simulations, including heat conduction, for a material described by an elastic/viscoplastic constitutive model that includes the effects of strain hardening, strain-rate hardening, and thermal softening. These simulations predict the propagation of a region of localized shearing deformation — a shear band — in front of the crack tip; however, the predicted shear band lengths are much less than those observed in the experiments. Numerical studies are presented to try to provide insight into the origins of this discrepancy.

## 1 INTRODUCTION

When cracks are subjected to shear wave loading the region in front of the crack tip may fail either by fracture or by the formation of a shear band. This competition between dynamic failure modes was highlighted by Kalthoff [1] in pioneering experiments on the edge impact of edge-notched steel plates to generate mode II loading at the notch-tip. He found that, for a maraging steel, failure occurred by fracture on a plane at approximately  $70^\circ$  from the initial crack plane when the impact velocities were relatively low, say  $10\text{ m/s}$ . However, at higher impact velocities, say greater than  $20\text{ m/s}$ , failure occurred by shear localization along a plane that is nearly parallel to the plane of the original crack. Mason *et al.* [2] conducted similar experiments and obtained similar results, while providing new information on the stress and deformation fields near the propagating shear band. Zhou *et al.* [3] extended the latter investigation to include measurements of temperature in the vicinity of the notch tip. For the maraging steel C-300 they found temperature increases of as much as approximately  $1400^\circ\text{C}$ , strongly suggesting that the observed shear bands result from a thermoplastic instability. In this steel they observed shear band speeds as high as  $1200\text{ m/s}$  at impact velocities of  $30\text{ m/s}$ . Zhou *et al.* [4] performed finite element simulations of their experiments and demonstrated remarkably good agreement between characteristic quantities of the experiments: temperature increases, shear band lengths, and shear band speeds.

Mode II experiments of the type just cited have done much to characterize the conditions associated with the generation of shear bands at crack tips. The current investigation was undertaken to advance this understanding by simplifying the loading conditions so that comparisons between theory and experiment could be made as directly as possible. Possible effects of wave reflections through the thickness of the steel plates in the experiments of Kalthoff [1], and others cited above, are eliminated by using a plate impact geometry to generate plane waves that are unaffected by lateral boundaries during the times of interest. By using a pressure-shear plate impact configuration it is possible to subject a mid-plane crack in the target plate to stress wave loading that is purely mode II or purely mode III --- or any combination of the two. In a previous paper Zhang and Clifton [5] presented results for the case of mode III loading for which the elastic wave analysis of the experiments is particularly straightforward and principal results had already been obtained in analytical form, e.g. Achenbach [6]. An important result of this analysis, which describes the propagation of a shear band in front of the crack tip, is that the predicted length of the band is much less than that observed in the experiments.

The plan of the paper is to provide first a brief description of the main results of the pressure-shear impact experiments for the case of Mode II loading. Then, to describe finite element simulations of the experiments that were intended to relate the observed response to predictions based on an elastic/viscoplastic model of the material response. Again, shorter shear bands are predicted than those observed in the

experiments. Further simulations to gain understanding of the sensitivity of the discrepancy to material and computational parameters are summarized briefly.

## 2 EXPERIMENTAL RESULTS

Scanning electron microscope images of post-impact samples indicate a long, thin, shear band extending forward from the tip of the crack as shown in Figures 1a and 1b. The shear band is the silky, darker gray region bounded by the lighter gray regions that constitute the original tempered martensite of AISI 4340 with its needle-like grains. The width of the band is approximately  $10\ \mu\text{m}$ . The cracks in and along the band are believed to be late-occurring artifacts associated with the arrival of a tensile wave reflected from the rear surface of the target plate. This belief is supported by the observation that such cracks are largely prevented when a momentum trap is placed at the back of the target plate to eliminate the reflected tensile pulse.

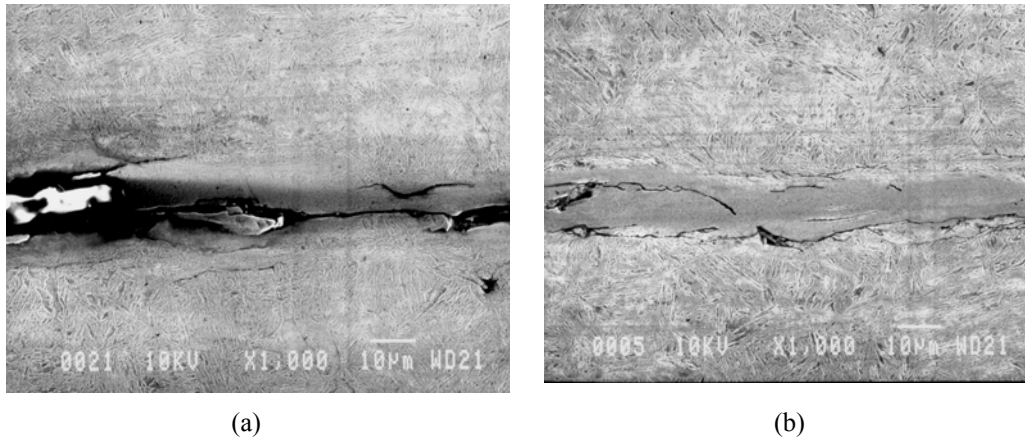


Figure 1: Cross-section of a shear band that propagated in front of a crack tip; (a) origin of the shear band at the tip of the pre-fatigue crack; (b) representative cross-section distant from the crack tip. (Impact velocity =  $125\ \text{m/s}$ ; Angle of inclination =  $18^\circ$ , Pulse duration =  $0.74\ \mu\text{s}$ ; Total length of shear band =  $1.4\ \text{mm}$ )

Velocity-time profiles of the rear surface motion of the target plate are shown in Figures 2a and 2b for a position that is approximately  $0.5\ \text{mm}$  in front of the edge of the crack, projected onto the rear surface. The normal velocity history shows a largely elastic initial longitudinal pulse followed by a lower amplitude pulse diffracted from the crack. The rounding at the top of the rising portion of the profile and the tail at the end of the initial pulse are indicators that some plastic deformation occurred. The transverse velocity history includes an initial transverse motion associated with a small inclination of the incident longitudinal wave relative to the normal to the rear surface. This inclination is due to a slight tilt (approximately  $0.8\ \text{milliradians}$ ) between the flyer plate and the target plate at impact. The incident plane shear wave arrives at  $t \approx 3.54\ \mu\text{s}$  and the returning longitudinal wave diffracted from the crack arrives at  $t \approx 3.60\ \mu\text{s}$  (See the t-X diagram in Figure 3; time axes in Figures 2 and 3 are shifted by approximately  $0.4\ \mu\text{s}$ ). Interpretation of the shear wave is further complicated by the incident diffracted shear wave arriving at approximately the same time. The diffracted longitudinal wave is responsible for the premature reduction in the transverse velocity – an effect that is further enhanced by the arrival of the plane unloading shear wave. There are indications of some inelastic response, at least in the vicinity of the crack tip, in the sense that the wavefronts are not as sharp as those predicted for purely elastic response. Detailed interpretation of the velocity-time profiles for the transverse velocity is made more difficult by the fact that the transverse motion at the rear surface depends on the location of the point of measurement relative to the crack-tip and the location of that position is difficult to control to an accuracy of better than, say,  $1\text{-}2\ \text{mm}$ .

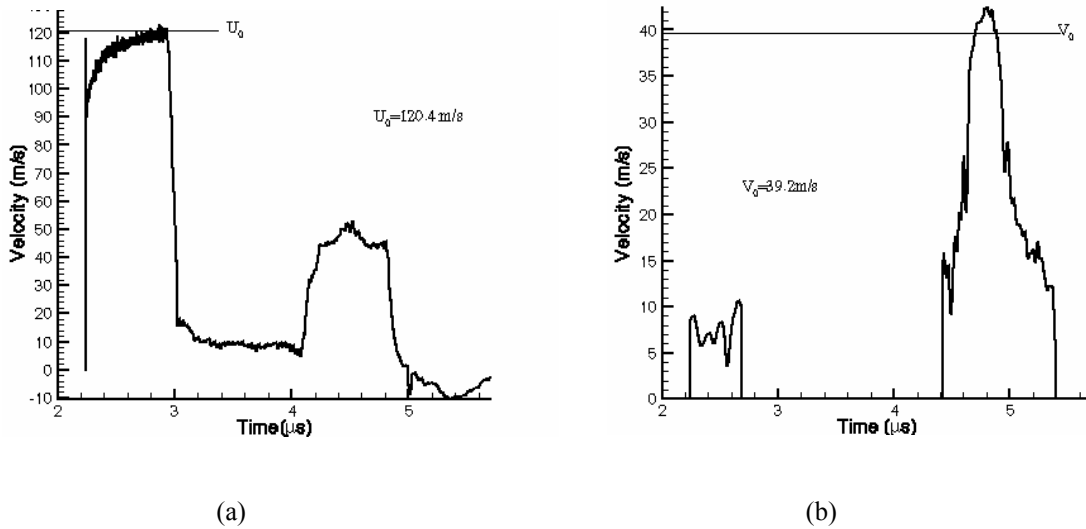


Figure 2: Velocity-time profiles for rear surface of pre-cracked plate subjected to Mode II loading in pressure-shear plate impact. (a) is the normal velocity and (b) is the transverse velocity in the direction of shearing; position of measurement is at a distance  $a \approx 0.5$  mm in front of the crack. (Impact velocity = 125 m/s; Angle of inclination =  $18^\circ$ , Pulse duration =  $0.75 \mu\text{s}$ ; tilt =  $0.8$  mrad)

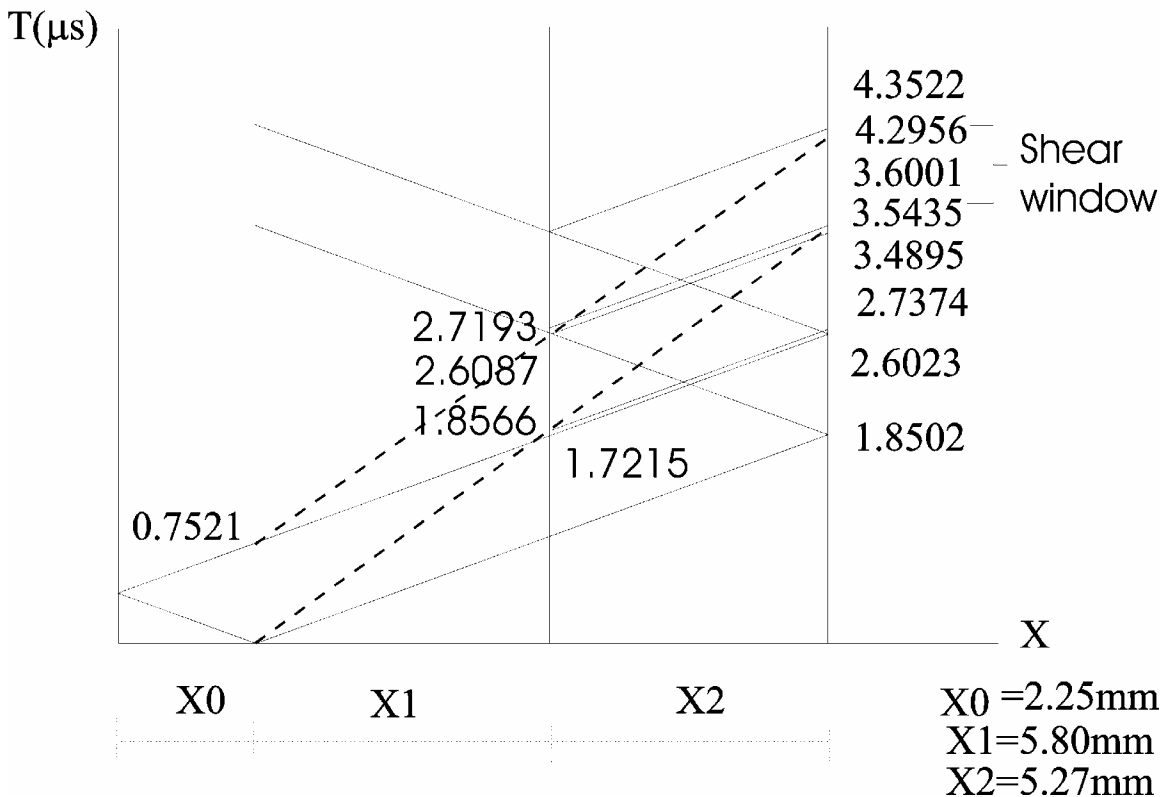


Figure 3: Plane wavefronts for pre-cracked plate subjected to Mode II loading in pressure-shear plate impact. (Impact velocity = 125 m/s; Angle of inclination =  $18^\circ$ , Pulse duration =  $0.75 \mu\text{s}$ ; Total length of shear band = 1.4 mm; longitudinal wave speed  $c_1 = 5.97$  km/s; shear wave speed  $c_2 = 3.12$  km/s.)

### 3 COMPUTER SIMULATIONS

In view of the evidence of shear bands, and the presence of wave profile features that appear to be related to plastic deformation of the material, it appears that the interpretation of these experiments requires a full elastic/viscoplastic analysis. For this analysis we use a simple power law model for the shearing resistance:

$$\tau = 1100 \left( \frac{\gamma^p}{0.005} \right)^n \left( \frac{\dot{\gamma}^p}{400} \right)^m \left( \frac{T}{298} \right)^\ell \quad (1)$$

where  $n=0.03$ ,  $m=0.02$  and  $\ell=-0.17$  are the exponents for the strain hardening, strain-rate hardening, and thermal softening, respectively. Parameter values are obtained from experimental data obtained by Tanimura and Duffy [7] and Clifton and Klopp [8] for AISI 4340 VAR steel under various tempering conditions. Interpolation of different yield stress values reported by Tanimura and Duffy [7] for different hardnesses suggests that, for a measured Rockwell Hardness of  $R_C = 52$  for the tempered 4340 used in the experiments reported herein, the value of 1100 MPa shown in Eqn. (1) is an appropriate flow stress in simple shear at the reference stain, strain-rate, and temperature shown in the denominators of (1).

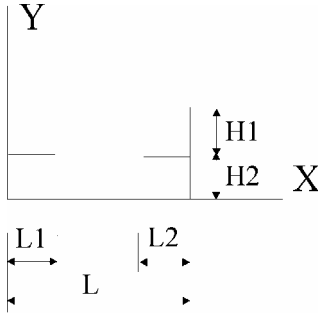


Figure 4: Model Geometry

Figure 4 shows the geometry of the pre-cracked plate for the FEM model used. The geometry is limited by the requirement that the region in front of the crack tip be unaffected by boundaries during the duration,  $t_0$ , of the initial pulse. This requirement is met for the geometry shown with  $L_1 = L_2 = H_1 = H_2 = (L/4) = c_1 t_0$ . To resolve details at length scales at, and below, the shear band thickness of  $10 \mu\text{m}$  (See Fig. 1), mesh sizes of  $5 \mu\text{m}$ ,  $2.5 \mu\text{m}$ , and  $1.25 \mu\text{m}$  were used. For these mesh sizes, supercomputer resources were required. The necessary resources were made available to run ABAQUS Explicit on the IBM p690 supercomputer from NCSA at UIUC. Even with these resources, memory limitations made it possible to run the simulations only for real time durations of  $t_0$ ,  $t_0/2$ , and  $t_0/4$ , respectively, for the successively smaller mesh sizes. Because temperature variations are important, coupled temperature-displacement elements were used. The fraction,  $\beta$ , of plastic work converted to heat was taken to be 0.9.

The boundary conditions on the boundaries  $x=0$  and  $x=L$  are taken to be the periodicity conditions:

$$u_i(0, y, t) = u_i(L, y, t), \quad i = 1, 2 \quad (2)$$

where  $u_1$ ,  $u_2$  are the displacements in the  $x$  and  $y$  directions, respectively. For symmetric impact, the velocities at the impact face are

$$\begin{aligned} v_1(x, 0, t) &= \frac{1}{2} v_0 \sin \theta \\ v_2(x, 0, t) &= \frac{1}{2} v_0 \cos \theta \end{aligned} \quad (3)$$

for  $0 \leq t \leq t_0$  where  $v_0$  is the projectile velocity, and  $\theta$  is the angle between the direction of flight of the projectile and the normal to the impact face. For  $t \geq t_0$  the impact face is taken to be traction-free. The rear surface of the plate (i.e.  $y = H_1 + H_2$ ) is traction-free. The crack surfaces,  $y = H_2$ ;  $(L/4) \leq |x - L/2| \leq (L/2)$ , are also taken to be traction-free except for  $t \leq H_2/c_1 + t_0$  when the crack is taken to be closed so that the compression wave passes through without being diffracted. Initially the cracked plate is taken to be at rest, and unstressed. The simulation begins when the incident shear wave, propagating in the positive  $y$ -direction, reaches the crack plane. The incident longitudinal wave is not considered in the simulations described here in order to focus attention on shear effects.

A contour plot of the shear strain  $E_{12}$  at  $t=0.74 \mu\text{s}$  is shown in Figure 5. Only the region near the crack tip at  $x=L_1$  is shown. Near the crack tip the relative displacement of the top and bottom faces of the crack is approximately 1 mesh size or  $5 \mu\text{m}$ . The strain in front of the crack tip is localized in a band with

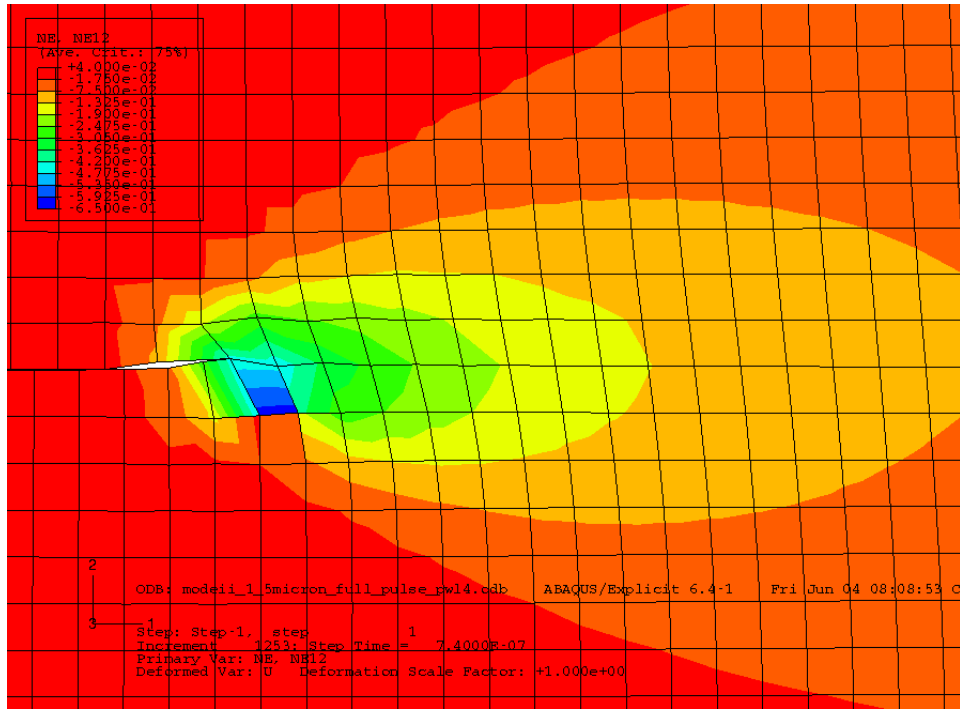


Figure 5: Nominal shear strain  $E_{12}$  at  $t = t_0 = 0.74 \mu s$  for a mesh size of  $5 \mu m$ .

thickness of approximately  $10\text{-}20 \mu m$ . However, the length of the band is less than  $50 \mu m$ , which is much less than the length of  $1.4 mm$  measured on the recovered samples. At positions in front of the crack tip the temperature distribution is nearly symmetrical with respect to the crack plane. The finite element calculations show the development of a narrow band of increased temperature extending forward from the crack tip. Details of the temperature distribution along the  $y$ -direction, at the crack tip, are shown in Figure 6a. The temperature distribution along the crack plane is shown in Figure 6b. As the mesh size is reduced the temperature rise becomes localized in a band with a width of approximately  $10 \mu m$ . The length of the region of sharply increasing temperature is less than  $30 \mu m$ . For each of the mesh sizes used the temperature at a fixed position increases essentially linearly with increasing time.

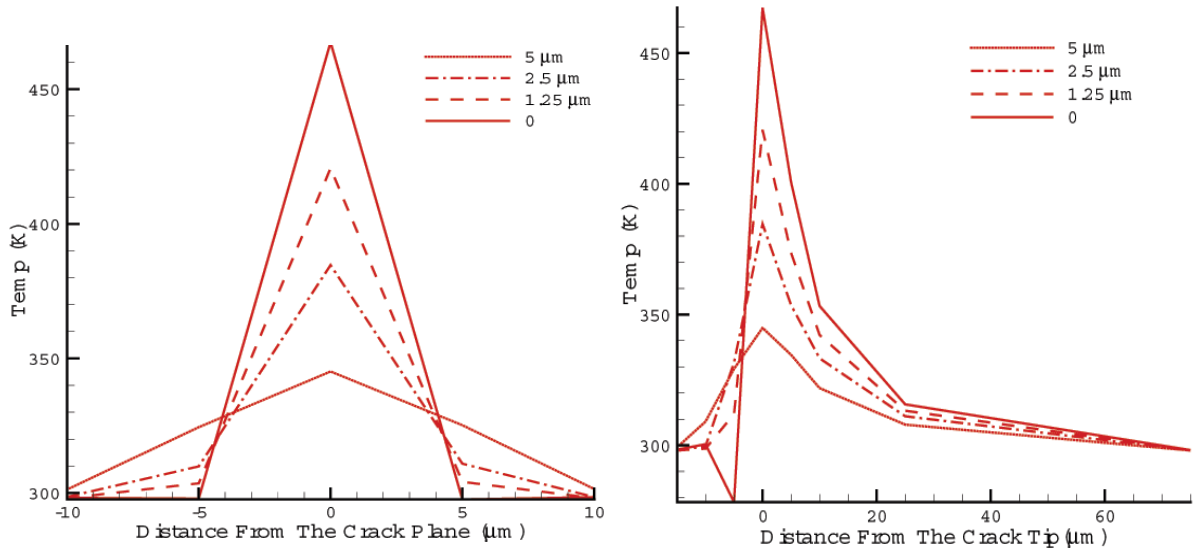


Figure 6: Temperature distributions at  $t = t_0/4$ : (a) perpendicular to the crack plane, at the crack tip; (b) along the crack plane. Extrapolated values for zero mesh size are obtained by fitting a cubic to results for the three mesh sizes shown and evaluating the cubic polynomial at zero mesh size.

## 4 DISCUSSION

The calculated rise in the temperature, and in the extension of the band, are considerably less than expected based on the experimental observation of long shear bands and evident changes in microstructure. To examine the possibility that the smaller calculated temperature rise results because the mesh size is not sufficiently small, simulations for the three different mesh sizes (i.e. 1.25, 2.5 and 5  $\mu m$ ) were used to obtain an extrapolated temperature distribution as the mesh size goes to zero. At  $t = t_0/4$  the maximum extrapolated temperature increase, which occurs at the crack tip, is approximately 170  $^{\circ}C$ . Because the temperature tends to increase essentially linearly with increasing time, the maximum extrapolated temperature rise at the end of the shear pulse is estimated to be approximately 680  $^{\circ}C$ , corresponding to a final temperature of approximately 700  $^{\circ}C$ . At these temperatures the flow stress for the material can be expected to be reduced substantially. Furthermore, the simulations with different mesh sizes indicate that the length of the band increases as the mesh size is reduced. However, it does not appear that the length of the band would be greater than, say, 400  $\mu m$ . Thus, the simulations do not appear to provide an explanation for the band lengths of approximately 1.4 mm observed in the experiments. Improved agreement can be obtained by reducing the strain hardening, reducing the strain-rate hardening, and increasing the thermal softening. However, simulations carried out to examine these effects indicate that the improvement obtained with a plausible range of parameter values (i.e.  $-0.68 \leq \ell \leq -0.17$ ,  $0 \leq m \leq 0.02$ ,  $-0.03 \leq n \leq 0.03$ ) does not provide sufficient change in the predicted results to obtain good agreement with experimental observations.

The lack of close agreement with the experimental results suggests that the power-law itself may not provide a sufficiently accurate model of the material response. Computational simulation of instability, such as the localization of the shearing deformation into a shear band, is sensitive to the details of the constitutive model and of the numerical methodology used in the simulation. In the simulations described here the tendency for instability may have been lessened by the lack of explicit consideration of the stability of the martensitic microstructure and by stabilizing features of the finite element modeling employed.

## 5 REFERENCES

1. Kalthoff, J.F., Shadow optical analysis of dynamic shear fracture, *Progr. Mater. Sci.* **814**, 531-538, 1987.
2. Mason, J.J., Rosakis, A.J., and Ravichandran, G., Full field measurements of the dynamic deformation field around a growing adiabatic shear band at the tip of a dynamically loaded crack notch, *J. Mech. Phys. Solids* **42**, 1679-1697, 1994.
3. Zhou, M., Ravichandran, G., and Rosakis, A., Dynamically propagating shear bands in impact-loaded investigation of temperature signatures and propagation speed, *J. Mech. Phys. Solids* **44**, 981-1006, 1996.
4. Zhou, M., Ravichandran, G., and Rosakis, A., Dynamically propagating shear bands in impact-loaded pre-notched plates — ii. Numerical simulations, *J. Mech. Phys. Solids* **44**, 1007-1032, 1996.
5. Zhang, Z. and Clifton, R.J., Shear band propagation from a crack tip, *J. Mech. Phys. Solids* **51**, 1903-1922, 2003.
6. Achenbach, J.D., Brittle and ductile extension of a finite crack by a horizontally polarized shear wave, *Int. J. Eng. Sci.* **8**, 947-966, 1970.
7. Tanimura, S., and Duffy, J., Strain-rate effects and temperature-history effects for three different tempers of 4340 VAR steels, *Int. J. Plasticity* **2**, 21-35, 1986.
8. Clifton, R.J. and Klopp, R., Pressure-shear plate impact testing, (in *Metals Handbook: Mechanical Testing, Vol. 8, 9<sup>th</sup> Edition*, American Society of Metals, Metals Park, OH), 25-38, 1985.

